Journal of Marine Research, 58, 609–630, 2000

Modeling $\delta^{15}N$ evolution: First palaeoceanographic applications in a coastal upwelling system

By Xavier Giraud[1], Philippe Bertrand[1], Véronique Garçon[2] and Isabelle Dadou[2]

ABSTRACT

The $\delta^{15}N$ signal in marine sediments appears to be a good palaeoceanographic tracer. It records biological processes in the water column and is transferred to and preserved in the sediments. Changes in forcing factors in upwelling systems may be recorded by $\delta^{15}N$. These forcing conditions can be of a biogeochemical nature, such as the initial isotopic signal of the nutrients or the trophic structure, or of a physical nature, such as wind stress, insolation, temperature or dynamic recycling.

A simple nitrogen-based trophic chain model was used to follow the development of the nitrogen isotopic signal in nutrients, phytoplankton, zooplankton and detritus. Detrital $\delta^{15}N$, influenced by the isotopic signature of the upwelled nutrients and isotopic fractionation along the trophic chain (photosynthesis and zooplankton excretion), was then compared to the sedimentary signal measured off Mauritania.

In our model, the biological variables are transported at shallow depths by a simple circulation scheme perpendicular to the coast depicting a continental shelf recirculation cell. Because cell length depends on the extension of the continental shelf, modifications of the cell length mimic sea level changes. Long cell length (high sea level) scenarios produce higher $\delta^{15}N$ values whereas short cell length scenarios result in lower values as in the glacial low sea level periods. Despite changes in many climatic parameters throughout this period, our results show that changing the sea level is sufficient to reconstruct the main pattern of the sedimentary $\delta^{15}N$ variations offshore of the Mauritanian upwelling, i.e. an increase from about 3‰ to 7‰ during the deglaciation, without invoking any change in nitrogen fixation or denitrification.

1. Introduction

$\delta^{15}N$ downcore measurements (on bulk sediment) in Mauritanian upwelling sediments (Fig. 1) show strong variations during glacial-interglacial stages and depict an increase during deglaciation (Martinez, 1997). Such variations have been related to changes in nutrient inventories or in denitrification rates in the global ocean (Calvert *et al.,* 1992, Altabet *et al.,* 1995, Farrell *et al.,* 1995). Some variations in the rates of denitrification and nitrogen fixation may have a significant impact on atmospheric CO_2 changes over glacial-interglacial periods through the primary production capability (Ganeshram *et al.,*

1. Dept. de Géologie et Océnographie, UMR 5805 EPOC, CNRS, Université de Bordeaux I, 33405 Talence, France. ***email: x.giraud@geocean.u-bordeaux.fr***

2. UMR 5566 LEGOS, CNRS, 18 Avenue Edouard Belin, 31401 Toulouse Cedex 4, France.

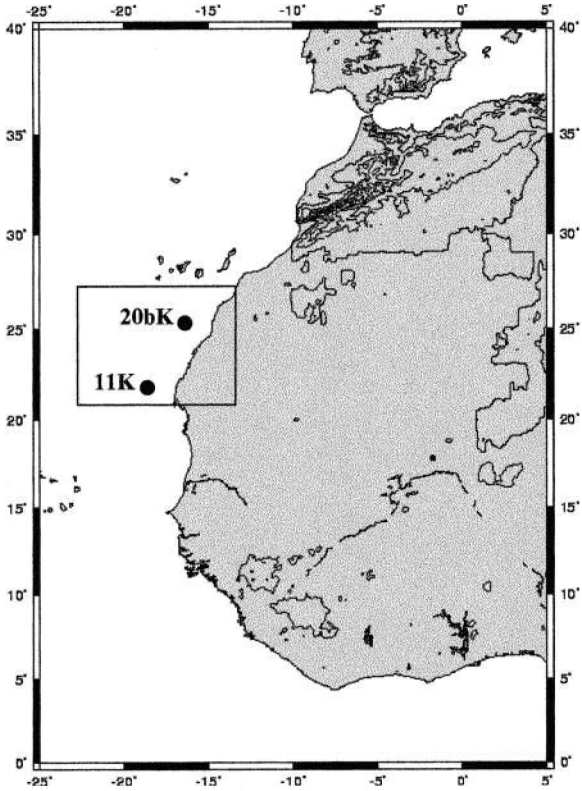

Figure 1. Location map of sedimentary cores. Core 11K, offshore of Cap Blanc (21°28.87′N; 17°57.35′W; 1200 m depth), and core 20bK (25°1.7′N; 16°39.2′W; 1450 m depth) were collected during the SEDORQUA cruise. Square inside is the study area of the Mauritanian upwelling.

1995; Falkowski, 1997). In this context, upwelling areas may be important in the mechanisms of global climate changes.

$\delta^{15}N$ has been described as an efficient palaeoceanographic tracer (François *et al.,* 1992; Altabet and François, 1994; Calvert *et al.,* 1995). This signal is generated by different isotope fractionations along the trophic chain in the near-surface waters and is transferred to the sediments. There is a strong relation between core top sediment $\delta^{15}N$ and the nitrate concentration in surface water, more specifically the degree of nitrate utilization (Altabet and François, 1994; Holmes *et al.,* 1996, 1998). In upwelling systems, the progression from eutrophic to oligotrophic conditions is related to NO_3 concentration and utilization.

In our study area, as organic matter is mainly of planktonic nature (Martinez, 1997), sedimentary $\delta^{15}N$ signal can be considered specific to the marine biological development and does not depend on the dilution by other fractions, either inorganic, detritic or aeolian input. Denitrification processes may also alter the nitrogen composition, but oxygen concentrations are too high for nitrate reduction to occur in the Mauritanian margin (Minas

et al., 1982). During the transfer from the surface ocean to the sea floor, isotopic signature of settling particles may change (Altabet, 1988; Voss *et al.,* 1996), probably due to bacterial degradation and/or trophic consumption. This possible transfer of isotopes due to trophic conditions in the water column is implicit in the biological trophic chain model. Moreover, at present, little diagenetic alteration has been observed (Altabet and François, 1994) and Martinez *et al.* (2000) did not find any significant downcore changes in $\delta^{15}N$ in the first centimeters of sediment.

The aim of this study is to understand the main mechanisms responsible for $\delta^{15}N$ variations in a coastal upwelling system using a biological model which includes isotope fractionation equations embedded in a simple circulation scheme. Bertrand *et al.* (2000) also used a conceptual model for both biological and 2D physical circulation processes to reconstruct $\delta^{15}N$ evolution along glacial-interglacial periods. Here we use a more realistic biological model describing an actual trophic chain. It is assumed that planktonic nitrogen fractionation processes do not change during glacial-interglacial periods. An upwelling circulation scheme, which transports the biological tracers, is developed to simulate the physical variations during glacial-interglacial stages. The paper is organized as follows: the biological model is described in Section 2. In Section 3, the simplified circulation scheme is presented. Results are described and discussed in Section 4 and conclusions follow in Section 5.

2. Biological model description

a. The NPZD model

The biological model we chose to adapt is a nitrogen-based model, which includes four components, namely nutrients (N), phytoplankton (P), zooplankton (Z) and a detritus pool (D) (Oschlies and Garçon, 1998, 1999; Fig. 2). The variations of nitrogen concentrations in each element are expressed in a system of four differential equations:

$$\frac{dN_P}{dt} = J(z, t, N_N)N_P - G(N_P)N_Z - \nu_P N_P \tag{1}$$

$$\frac{dN_Z}{dt} = \gamma_1 G(N_P)N_Z - \gamma_2 N_Z - \nu_Z N_Z^2 \tag{2}$$

$$\frac{dN_D}{dt} = (1 - \gamma_1)G(N_P)N_Z + \nu_P N_P + \nu_Z N_Z^2 - \nu_D N_D - \omega_D N_D \tag{3}$$

$$\frac{dN_N}{dt} = \nu_D N_D + \gamma_2 N_Z - J(z, t, N_N)N_P \tag{4}$$

where N_i and dN_i/dt are the concentration (of nitrogen) and the variation of the concentration over time for the component i, respectively. The different terms of these equations express phytoplankton growth rate, grazing of phytoplankton by zooplankton (with

Table 1. Parameters of the biological model (Oschlies and Garçon, 1999). Parameters have been adjusted over the North Atlantic Ocean by comparison with time series station data.

Parameter	Symbol	Value
Phytoplankton coefficients		
Initial slope of P-I curve	α	$0.025\ (\mathrm{W\ m^{-2}})^{-1}\ \mathrm{d^{-1}}$
Light attenuation due to water	k_w	$0.04\ \mathrm{m^{-1}}$
Maximum growth rate parameters	a	$0.6\ \mathrm{d^{-1}}$
	b	1.066
	c	$1.0\ (^\circ\mathrm{C})^{-1}$
Half-saturation constant for N uptake	k_1	$0.5\ \mathrm{mmol\ m^{-3}}$
Specific mortality rate	v_P	$0.03\ \mathrm{d^{-1}}$
Zooplankton coefficients		
Assimilation efficiency	γ_1	0.75
Maximum grazing rate	g	$2.0\ \mathrm{d^{-1}}$
Prey capture rate	ε	$1.0\ (\mathrm{mmol\ m^{-3}})^{-2}\ \mathrm{d^{-1}}$
Quadratic mortality†	v_Z	$0.20\ (\mathrm{mmol\ m^{-3}})^{-1}\ \mathrm{d^{-1}}$
Excretion	γ_2	$0.03\ \mathrm{d^{-1}}$
Detrital coefficients		
Remineralization rate	v_D	$0.05\ \mathrm{d^{-1}}$
Export rate	ω_D	$0.5\ \mathrm{d^{-1}}$

Photosynthesis and grazing expressions

Photosynthesis growth rate

$$J(z, t, N_N) = \min\left(J(z, t), J_{\max}\frac{N_N}{k_1 + N_N}\right)$$

Growth rate without nutrient limitation

$$J(z, t) = \frac{J_{\max}\alpha I(z, t)}{[J_{\max}^2 + (\alpha I(z, t))^2]^{1/2}}$$

Maximum growth rate

$$J_{\max} = ab^{CT}$$

Insolation

$$I(z, t) = I(t)_{z=0}\exp\left(k_w z/(1 - (\cos\theta/1.33)^2)^{1/2}\right)$$

Zooplankton grazing expression

$$G(N_P) = \frac{g\varepsilon N_P^2}{g + \varepsilon N_P^2}$$

where: min (x, y) is the function "minimum,"
z is depth, (in m)
t is time,
T is temperature (°C)
and θ is the angle of incidence at noon (in radian)

†Zooplankton quadratic mortality term represents increasing populations of predators as zooplankton populations increase and is more stable than a linear term (Steele and Hederson, 1992; Evans, 1999).

assimilation efficiency), mortality of phytoplankton and zooplankton, excretion of zooplankton and remineralization of detritus to nutrients (see Table 1 for further details and parameter values). The model can be used throughout the water column: in the surface layer, light allows photosynthetic growth and, therefore, the development of all trophic

levels; while in the deeper layers, the lack of light stops this primary production and only degradation and remineralization may occur.

As our purpose is to compare sedimentary data with the model outputs, the model also considers a term of detritus export from the euphotic layer, sinking through the water column to the bottom, expressed as $\omega_D N_D$ (Eq. 3). ω_D has the dimension of a vertical velocity V (of a sinking particle) divided by the euphotic layer depth H. We chose a typical H equal to 20 m (Babin *et al.,* 1996) and a typical V of 10 m d^{-1} (Alldredge and Gotschalk, 1988; Wefer and Fischer, 1993) yielding a rate of 0.5 d^{-1} for ω_D.

The addition of the $\delta^{15}N$ computation for each biological component yields a doubling of the number of biological state variables. This will greatly increase the computation time when coupling this module into a complex physical code. The objective here was to build an investigation tool to swiftly test various oceanographic and climatic scenarios. This justifies the use of a simple initial biological model as this *NPZD* one.

b. *Computation of the* $\delta^{15}N$

The fractionation of nitrogen isotopes is responsible for the differences between the $\delta^{15}N$ signatures of the four biological components. Phytoplankton photosynthesis and zooplankton excretion are two important processes during which fractionation occurs. Remineralization fractionation is not dealt with to keep the model simple. We intentionally chose a simple biological model and chose not to integrate such a fractionation feature like bacterial degradation. The fractionation that may occur during the formation of fecal pellets produced by marine zooplankton is questionable. According to Montoya (1994), the difference between the fecal pellets $\delta^{15}N$ and the animal $\delta^{15}N$ ranges between $-3.7‰$ and $4.8‰$. We will therefore only consider phytoplankton photosynthesis and zooplankton excretion fractionation processes.

During photosynthesis, the lighter isotope (^{14}N) is thermodynamically preferred to the heavier (^{15}N) for incorporation into the new tissues. This is expressed as follows (Altabet *et al.,* 1995):

$$\delta^{15}N_{\text{new POM}} = \delta^{15}N_N - \varepsilon \tag{5}$$

where $\delta^{15}N_{\text{newPOM}}$ is the isotopic signature of the new particulate organic matter (in ‰), $\delta^{15}N_N$ the isotopic signature of the nutrients (in ‰) and ε is the enrichment factor associated with phytoplankton uptake (in ‰). Waser *et al.* (1998) estimated the value of ε to be $5.2‰$ when nitrates are used as the substrate in primary production.

The fractionation equation for zooplankton excretion is expressed in the same form:

$$\delta^{15}N_{\text{exc}} = f'\delta^{15}N_Z - \varepsilon' \tag{6}$$

where $\delta^{15}N_{\text{exc}}$ is the isotopic signature of the excretion product (in ‰) and $\delta^{15}N_Z$ is the isotopic signature of zooplankton (in ‰). The fractionation equation is a linear regression (Checkley and Miller, 1989) with the slope of the curve $f' = 0.96$ and $\varepsilon' = 2.7‰$. Nitrogen isotope fractionation by zooplankton during excretion is the process responsible for the stepwise enrichment of ^{15}N along the trophic chain, in our case between phytoplankton and

zooplankton. This ^{15}N enrichment has been measured as 3.4‰ (DeNiro and Epstein, 1980; Minagawa and Wada, 1984).

The initial biological model considers the fluxes of total nitrogen, ^{14}N plus ^{15}N. To model the variations of $\delta^{15}N$, we need to follow the transfers of ^{15}N separately.

Let's consider the photosynthesis fractionation. Let N_{JP} equal the total nitrogen quantity transferred from nutrients to phytoplankton; it is also JN_P and includes ^{14}N and ^{15}N:

$$N_{JP} = {}^{15}N_{JP} + {}^{14}N_{JP}. \tag{7}$$

According to Eq. (5), the $\delta^{15}N$ of what is transferred is:

$$\delta^{15}N_{JP} = \delta^{15}N_N - \varepsilon. \tag{8}$$

With the $\delta^{15}N$ definition:

$$\delta^{15}N = [(^{15}N/^{14}N)_{\text{sample}}/(^{15}N/^{14}N)_{\text{standard}} - 1] \times 1000, \tag{9}$$

it follows that:

$$\frac{^{15}N_{JP}}{^{14}N_{JP}} = \frac{^{15}N_N}{^{14}N_N} - \frac{\varepsilon R_{\text{std}}}{1000}, \tag{10}$$

where $R_{\text{std}} = (^{15}N/^{14}N)_{\text{standard}} = 0.3663/99.6337$ is the standard ratio of the ^{15}N and ^{14}N nitrogen isotopes in air (Fogel and Cifuentes, 1993). All elements of the right-hand side are known quantities. It can be reformulated as follows:

$$^{15}N_{JP} = \beta\,{}^{14}N_{JP}, \tag{11}$$

with

$$\beta = \frac{^{15}N_N}{^{14}N_N} - \frac{\varepsilon R_{\text{std}}}{1000}. \tag{12}$$

Eqs. (7) and (11) give:

$$^{15}N_{JP} = \frac{\beta}{1+\beta} N_{JP} = \frac{\beta}{1+\beta} JN_P. \tag{13}$$

This $^{15}N_{JP}$ is equivalent to the quantity of ^{15}N that is transferred from nutrients to phytoplankton during photosynthesis. The phytoplankton ^{15}N stock ($^{15}N_P$) will be increased by this quantity and by analogy with Eq. (1) we obtain:

$$\frac{d\,^{15}N_P}{dt} = \frac{\beta}{1+\beta} J(z, t, N_N) N_P + \cdots \tag{14}$$

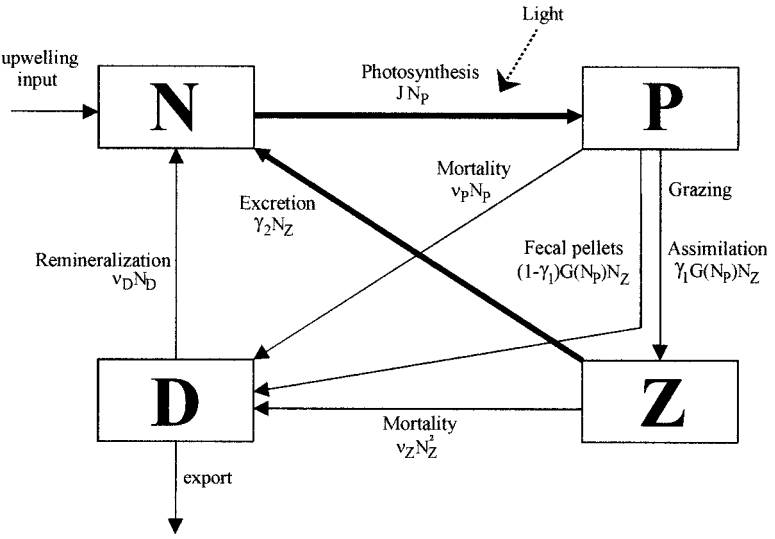

Figure 2. Scheme of the biological model (Oschlies and Garçon, 1999). Parameters of the fluxes between Nutrients, Phytoplankton, Zooplankton and Detritus are expressed in Table 1. Bold arrows represent the two main important isotope fractionation processes that we consider, i.e. phytoplankton photosynthesis and zooplankton excretion.

Now let's consider the transfer of nitrogen between the phytoplankton and the detritus because of mortality of the former, N_{PD}, which is also $v_P N_P$ (cf. Fig. 2).

$$N_{PD} = {}^{15}\mathrm{N}_{PD} + {}^{14}\mathrm{N}_{PD} = {}^{15}\mathrm{N}_{PD}\left(1 + \frac{1}{{}^{15}\mathrm{N}_{PD}/{}^{14}\mathrm{N}_{PD}}\right). \tag{15}$$

As there is no fractionation during this transfer, the isotopic ratio of what is transferred is the same as the ratio of the phytoplankton it is coming from. It can be written as:

$$\frac{{}^{15}\mathrm{N}_{PD}}{{}^{14}\mathrm{N}_{PD}} = \frac{{}^{15}\mathrm{N}_{P}}{{}^{14}\mathrm{N}_{P}}. \tag{16}$$

With (15) and (16) we have:

$${}^{15}\mathrm{N}_{PD} = \frac{{}^{15}\mathrm{N}_{P}}{{}^{15}\mathrm{N}_{P} + {}^{14}\mathrm{N}_{P}}\,\nu_P \mathrm{N}_P; \tag{17}$$

but

$${}^{15}\mathrm{N}_{P} + {}^{14}\mathrm{N}_{P} = N_P, \tag{18}$$

so

$${}^{15}\mathrm{N}_{PD} = \nu_P\,{}^{15}\mathrm{N}_{P}. \tag{19}$$

This $^{15}N_{PD}$ corresponds to the quantity of ^{15}N that is transferred from phytoplankton to detritus because of the phytoplankton mortality. Continuing the analogy with Eq. (1), we have:

$$\frac{d^{15}N_P}{dt} = \frac{\beta}{1+\beta} J(z, t, N_N) N_P - \nu_P {}^{15}N_P + \cdots \tag{20}$$

We considered both ways of transfer of nitrogen, with and without isotopic fractionation. Other exchanges can be treated accordingly to obtain the following system of equations:

$$\frac{d^{15}N_P}{dt} = \frac{\beta}{1+\beta} J(z, t, N_N) N_P - \nu_P {}^{15}N_P - \frac{{}^{15}N_P}{N_P} G(N_P) N_Z \tag{21}$$

$$\frac{d^{15}N_Z}{dt} = \frac{{}^{15}N_P}{N_P} \gamma_1 G(N_P) N_Z - \frac{\beta'}{1+\beta'} \gamma_2 N_Z - \nu_Z {}^{15}N_Z^2 \tag{22}$$

$$\frac{d^{15}N_D}{dt} = \frac{{}^{15}N_P}{N_P} (1-\gamma_1) G(N_P) N_Z + \nu_P {}^{15}N_P + \nu_Z {}^{15}N_Z^2 - \nu_D {}^{15}N_D - \omega_D {}^{15}N_D \tag{23}$$

$$\frac{d^{15}N_N}{dt} = \nu_D {}^{15}N_D + \frac{\beta'}{1+\beta'} \gamma_2 N_Z - \frac{\beta}{1+\beta} J(z, t, N_N) N_P \tag{24}$$

3. The simplified circulation scheme

a. Description of the upwelling recirculation

The Scientific Committee on Oceanographic Research (SCOR, 1975) described different kinds of coastal upwelling circulation schemes (Fig. 3). We will first focus on the scheme with a large shallow continental shelf, as in the Mauritanian type. It consists of a two-cell circulation, separated by a weak front. In a numerical study of the physical processes of the upwelling, Werner (1987) associates this front with the presence of the shelf break. Other authors also ascribe an important role of the shelf break location on the circulation (Neumann, 1968; Pietrafesa, 1983). Chen and Wang (1990) describe such a double cell circulation and ascribe the front formation to the deepening of the surface mixed layer. Smith (1995) describes the formation of the fronts in the coastal zone and their offshore migration. He does not associate them with the location of the shelf break but with the conflict between cold upwelled waters and warmer offshore waters. Whatever its origin, a recirculation cell seems to be located on the continental shelf. This cell is very important because it will contribute to the recirculation of detritus and nutrients in the upwelling. The remineralization of detritus will increase the quantity of nutrients available at the upwelling emergence zone and, therefore, increase the productivity. According to the schemes in Figure 3, such a cell does not exist for other upwelling types. The difference lies in the shelf and slope profiles: in the Oregon upwelling type (Fig. 3b), because the shelf slope is steeper than off Mauritania, the continental shelf is shorter. In this circulation

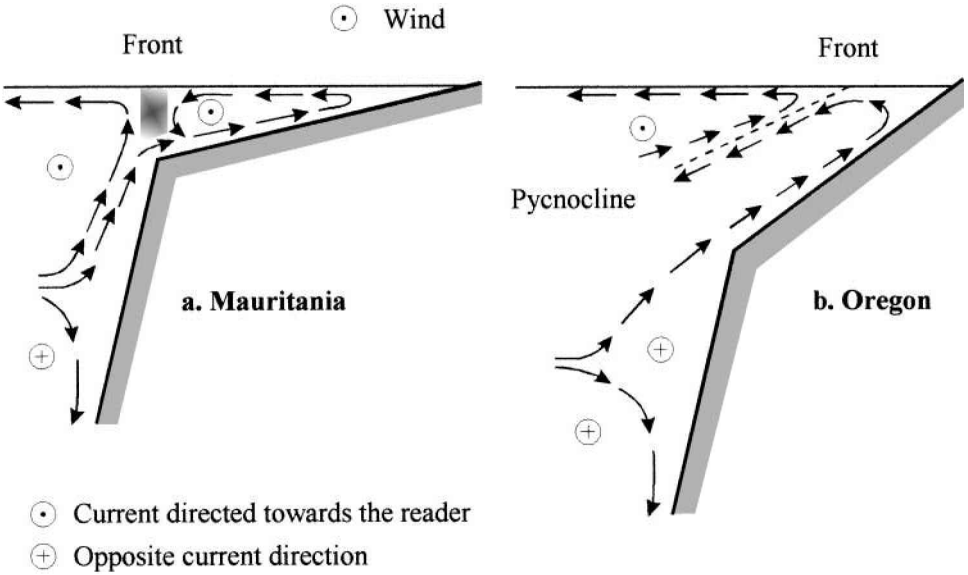

Figure 3. Coastal upwelling circulation schemes (SCOR, 1975) for Mauritania and Oregon. Those schemes are valid for the Northern Hemisphere, with a wind blowing from the north. The Oregon circulation type can be the circulation that occurs in the Mauritanian margin during low sea level stands due to the decrease of the shelf width. As we are interested in different sea level scenarios, our shelf configuration will balance between the two circulation types: a long recirculation cell like the Mauritanian margin for the high sea level (a) and no recirculation cell like the Oregon margin for the low sea level scenarios (b).

configuration, the cycling of detritus and nutrients back to the upwelling emergence point is less pronounced.

The comparison between the different upwelling schemes fits into the discussion on sea level change effects. Variations of sea level during the glacial-interglacial cycles will affect the bathymetry of the upwelling zones. Lower sea level should result in a narrower continental shelf off Mauritania, with circulation characteristics closer to the Oregon type. The percentage of recycling will be different, depending on the upwelling cell length. A long recirculation cell characterizes high sea level scenarios of interglacial stages whereas a short recirculation cell characterizes low sea level scenarios of glacial stages.

In order to study sea level effect alone, we will assume all the other parameters to be constant. The insolation and the surface current speed will not change in the different runs. The goal of this study is to understand the impact of the recirculation cell length on the biological development and the sedimentary $\delta^{15}N$ signal. First this recirculation cell will be simulated only by export of detritus during the transport offshore from the emergence point. In a second step, Section 4d, a sensitivity test on the recycling percentage is performed by increasing the export rate at the front location, depicting vertical velocities that close the continental shelf cell.

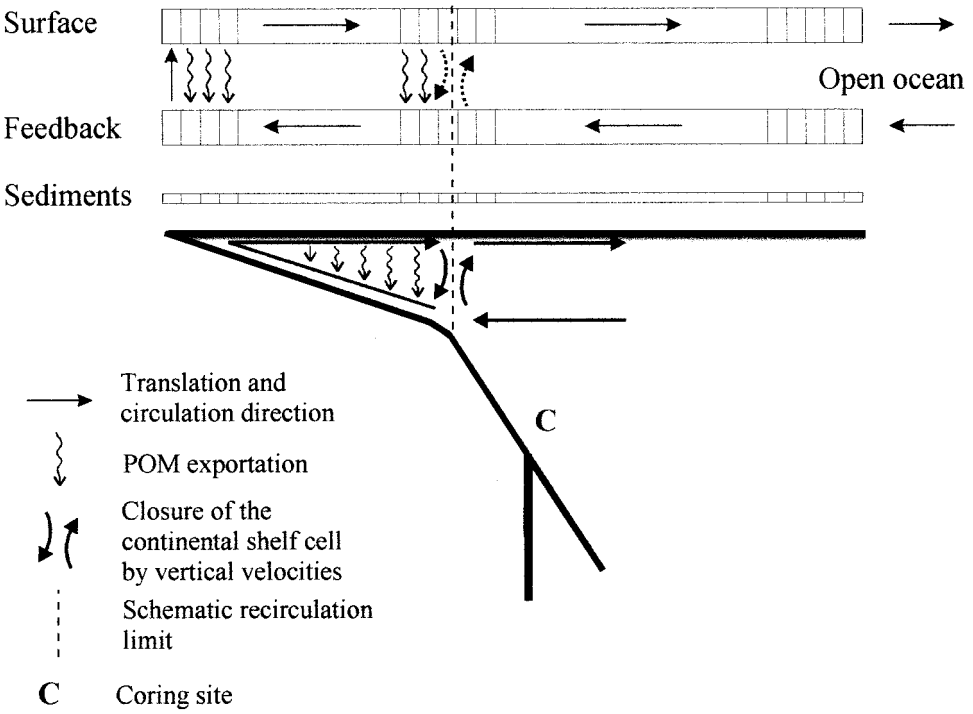

Figure 4. Representation of the numerical upwelling circulation scheme.

b. Upwelling circulation numerical set up

The aim of the physical representation is to allow the biological development in a surface layer, an export of the organic matter to a deeper layer where remineralization can occur and a reinjection of this deep layer to an upwelling emergence point (Fig. 4). We setup a type of conveyor belt, perpendicular to the coast, with a row of boxes depicting the surface euphotic layer and a second row for the deep aphotic layer. The development of the biological system is regularly computed in each box, taking into account its depth for the light availability. A simple translation movement from box to box imposes the circulation: offshore in the surface row and inshore in the deep row. The connection between the two layers at the first box of each row induces an upwelling emergence point. As the current speeds are weaker in the bottom layer than in the surface one, we set three times as many boxes in the deep row than in the surface one. This aspect is important for the remineralization time scale of the detritus. The surface layer is set at 20 m deep, which corresponds to the depth of the euphotic layer in an eutrophic zone (Babin *et al.,* 1996). The sea-surface temperature is held constant (at 18°C; Mittelstaedt, 1991) along the offshore transect. The hydrological characteristics of the deep row are those of a layer at about 200 m depth, with a mean temperature of 10°C (Fraga, 1974).

c. Coupling with the biological variables

In the model, the biological variables are continuously injected at the most offshore box of the deep row, with intermediate water characteristics. They are progressively transported shoreward to the upwelling emergence point. In the surface layer, light allows primary production and subsequent development of the biological loop. The latter occurs during the offshore transport. During the offshore transport, only a fraction of the detritus pool will sink and be exported to the deep layer. Presently the closure of the continental shelf cell by vertical velocities (Fig. 4) is not considered. Incorporating it will be further investigated (Section 4d). To simulate the upwelling cell, this exported matter is added to the corresponding underlying boxes, but only to a certain offshore limit. Beyond this limit, export from the surface layer proceeds but is no longer taken up, considering no further effect of recirculation at greater depths. All the nitrogen advected or exported beyond this limit is considered to be lost to the upwelling system. It is compensated by the inflow in the deep layer. Phytoplankton and zooplankton do not exist in the deep row where only detritus and nutrients are transported. Therefore, only nutrients and detritus arrive at the emergence point. To initiate the biological development in the surface layer, phytoplankton and zooplankton concentrations need to be specified at the upwelling emergence point. To simulate any lateral input, we continuously add low values of phytoplankton and zooplankton concentrations to the first box of the surface row before it is transported offshore. These values correspond to an oligotrophic equilibrium.

Considering the above discussion of the sea level change impact on the upwelling circulation, the positioning of the recirculation limit with respect to the upwelling emergence point will simulate the different sea level scenarios. At first order, we can consider that the farther offshore this limit is, the longer the upwelling coastal cell is, corresponding to a higher sea level situation. On the contrary, a short distance between the upwelling emergence point and the recirculation limit will simulate a low-stand sea level or an Oregon circulation type.

To build the record of the detritus $\delta^{15}N$, the sum of the ^{15}N and ^{14}N of the detritus is kept at each time step in a fictitious sedimentary row. As advection and resuspension of organic matter in the bottom boundary layer may homogenize the signal for each location, we will consider the upstream cumulative production of the detritus and its $\delta^{15}N$ signature. In the model, there is no interaction between the deep row and the sedimentary row. The quantity of organic matter found in the sediments is only a very small percentage of the primary production, leading us to consider that this sediment recording has no effect on the detritus concentration in the water column. It will not change the mass balance of the biological fields.

d. Initial and boundary conditions

Since the upper layer is 20 m deep, light conditions available are considered to be those prevailing at 10 m depth. Initial conditions for biological variable concentrations are

typical of an oligotrophic equilibrium, with only 10^{-2} mmol N m^{-3} for the N state variable (Babin *et al.,* 1996).

In the deep conveyor row, we set initial conditions for nutrients to a value of 10 mmol N m^{-3} (Jacques and Tréguer, 1986; Babin *et al.,* 1996) and phytoplankton, zooplankton and detritus to zero. These values are also characteristics of the intermediate waters injected into the system. The $\delta^{15}N$ of those nutrients is set to 6‰ (Altabet and Curry, 1989; Liu and Kaplan, 1989; Montoya, 1994).

4. Results and discussion

a. Biological development and $\delta^{15}N$ variations in the reference run

In order to simulate an actual situation, we assume a cell length of 100 km. With a surface current speed of 10 cm s^{-1} (Mittelstaedt, 1991), this distance corresponds to a development time of the biological tracers of about 12 days. This means that, starting from the emergence point of the upwelling, any matter exported from the surface layer will be added to the bottom layer, until this limit of 100 km—or 12 days. Beyond this limit, we are farther from the front and the system is just advected offshore. Figure 5 shows the curves of the biological variables in this case, in the surface row. In this run, the export rate of the detritus is 0.5 d^{-1}.

Nutrient concentration at the emergence point (0 km) is 18.7 mmol N m^{-3} whereas the quantity injected into the system in the bottom layer is 10 mmol N m^{-3}. The percentage of recycling is, therefore, about 87%, which is consistent with the value calculated by Jacques and Tréguer (1986) for nitrates. Availability of these nutrients allows an increase in phytoplanktonic biomass. Nutrients decrease whereas phytoplankton increases. According to Eq. 5, the isotopic signature of phytoplankton is about 5‰ lower than the nutrient isotopic value. As nutrients become more depleted, their isotopic signature increases and tends to infinity when nutrient concentration tends to zero. This is a limitation to the Rayleigh fractionation equation. When nutrients are fully depleted after about 32 km (3.75 days), the total nitrogen of the nutrients is in phytoplanktonic form. Phytoplankton has, therefore, the same isotopic ratio as the initial upwelled nitrates, at about 6‰. Because of an input of nutrients coming from the detritus remineralization, the nutrient isotopic signature is no longer infinite. The nutrient $\delta^{15}N$ remains heavy because of a high degree of nitrate utilization. The zooplankton biomass increases, following the phytoplankton bloom, and decreases by mortality during the offshore transport to reach oligotrophic conditions. Both phytoplankton and zooplankton contribute to the detritus pool in concentration and $\delta^{15}N$ signature. This increase of the detritus pool is responsible for the partial regeneration of the nutrients through remineralization. Because of this higher quantity of nutrients, the nitrate isotopic signature decreases. The new subsequent $\delta^{15}N$ increase is due to the consumption of nutrients. Finally, with the detritus export, all pools decrease during the offshore transport to reach oligotrophic conditions. However detritus $\delta^{15}N$ is always lower than the mean $\delta^{15}N$ value of the system. This leads to the fact that export of detritus out of the system will increase the $\delta^{15}N$ of the remaining biological variables. In this long cell length scenario, this effect is weak because the difference between the detritus $\delta^{15}N$

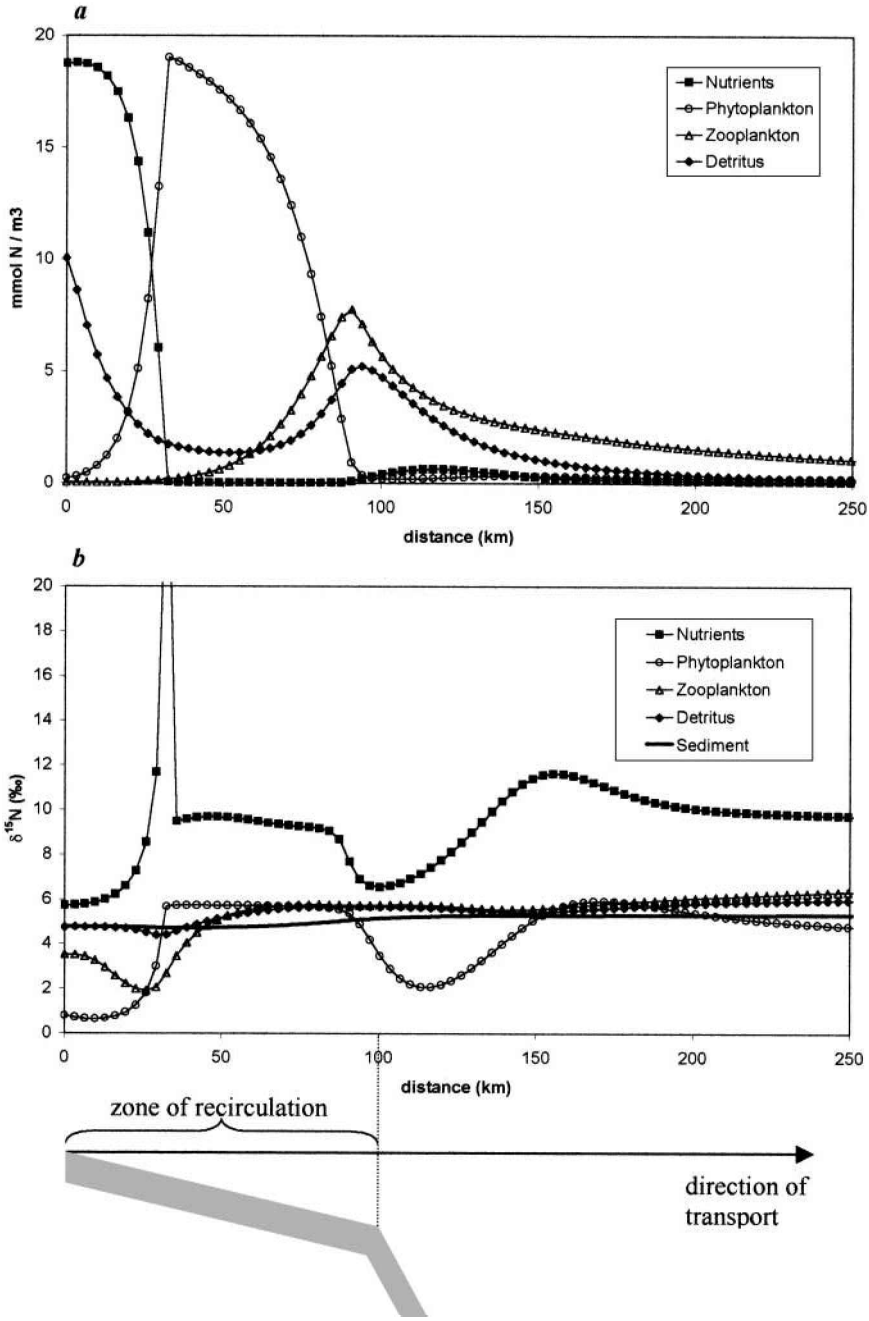

Figure 5. Evolution of the biological variables in an actual configuration from the emergence point to the offshore. The cell length for the recirculation is 100 km. (a) Evolution of the concentrations, in mmol N m^{-3}. (b) Evolution of the $\delta^{15}N$, in ‰. The scheme at the bottom puts the above curves into the context of the upwelling transect by showing the distance where the shelf recirculation occurs.

and the whole $\delta^{15}N$ is insignificant. This long recirculation distance is also responsible for the recycling of a large amount of detritus. Detritus $\delta^{15}N$ at the emergence point is therefore a mean of all values along the cell length as a result of homogenization. The resulting curve for the sediment $\delta^{15}N$ is almost flat along the transect, reaching a value of 5.3‰. This value corresponds to the equilibrium of the system after the planktonic bloom.

b. Sea level change scenarios

In order to consider a low sea level scenario, we study a no recirculation case (Fig. 6). In this case, nutrient concentration at the emergence zone is equal to the concentration injected in the bottom offshore box, i.e. 10 mmol N m^{-3}. The phytoplankton biomass increase is, therefore, weaker than in the previous case. Detritus $\delta^{15}N$ progressively increases up to a value of 5.6‰. As no recirculation is allowed, detritus cannot return to the upwelling emergence point. There is no homogenization effect and the $\delta^{15}N$ of phytoplankton and detritus at the beginning of the upwelling remains 5.2‰ lower than the nutrients $\delta^{15}N$. The resulting curve is a sigmoid from the emergence point to the offshore.

Figure 7 synthesizes the curves of the sediment $\delta^{15}N$ for intermediate cell lengths. From 100 to 40 km, $\delta^{15}N$ progressively decreases. Initial values drop because the homogenization effect is less and less important. From 40 to 0 km, this drop of initial values continues but the rest of the curve takes higher values. This is due to the export of detritus, which is lighter than the rest of the system. For low sea level scenarios, this effect is more important and produces an increase in the final asymptotic value of detritus $\delta^{15}N$.

Sensitivity tests performed to study the influence of the export rate ω_D confirm the different impact of the export for the small and long cell length scenarios (Fig. 8). The difference depends on the timing between the maximum development of the biological variables and the export limit of the detritus. For short cell length scenarios, detritus $\delta^{15}N$ is not at equilibrium with the rest of the system beyond the recycling zone. Past this limit, light compounds are exported and the final value of the detritus $\delta^{15}N$ is higher. On the contrary, for long cell length scenarios, export inshore of the limit of the cell homogenizes the detritus and the detritus that comes out of the recycling zone has reached the equilibrium value. The export rate has a homogenization effect but does not act on the final $\delta^{15}N$ asymptotic value. Recycling percentages vary from 40% (for an export rate ω_D of 0.2 d^{-1}) to 114% (ω_D at 0.75 d^{-1}), as compared to the 87% standard recycling rate.

For the model in the interglacial stage configuration (high sea level, cell length of 100 km, detritus export rate of 0.5 d^{-1}), the plateau value of 5.3‰ seems to be the maximum value that can be reached by the sediment $\delta^{15}N$. Whatever the position of the coring site relative to the coast, the sediment $\delta^{15}N$ predicted by the model ranges between 4.7 and 5.3‰. On the contrary, a glacial stage scenario, with a low stand sea level, provides lower values near the emergence point of the upwelling, around 0.8‰. This situation quickly evolves to reach higher values farther offshore, similar to the high sea level scenario, around 5.6‰.

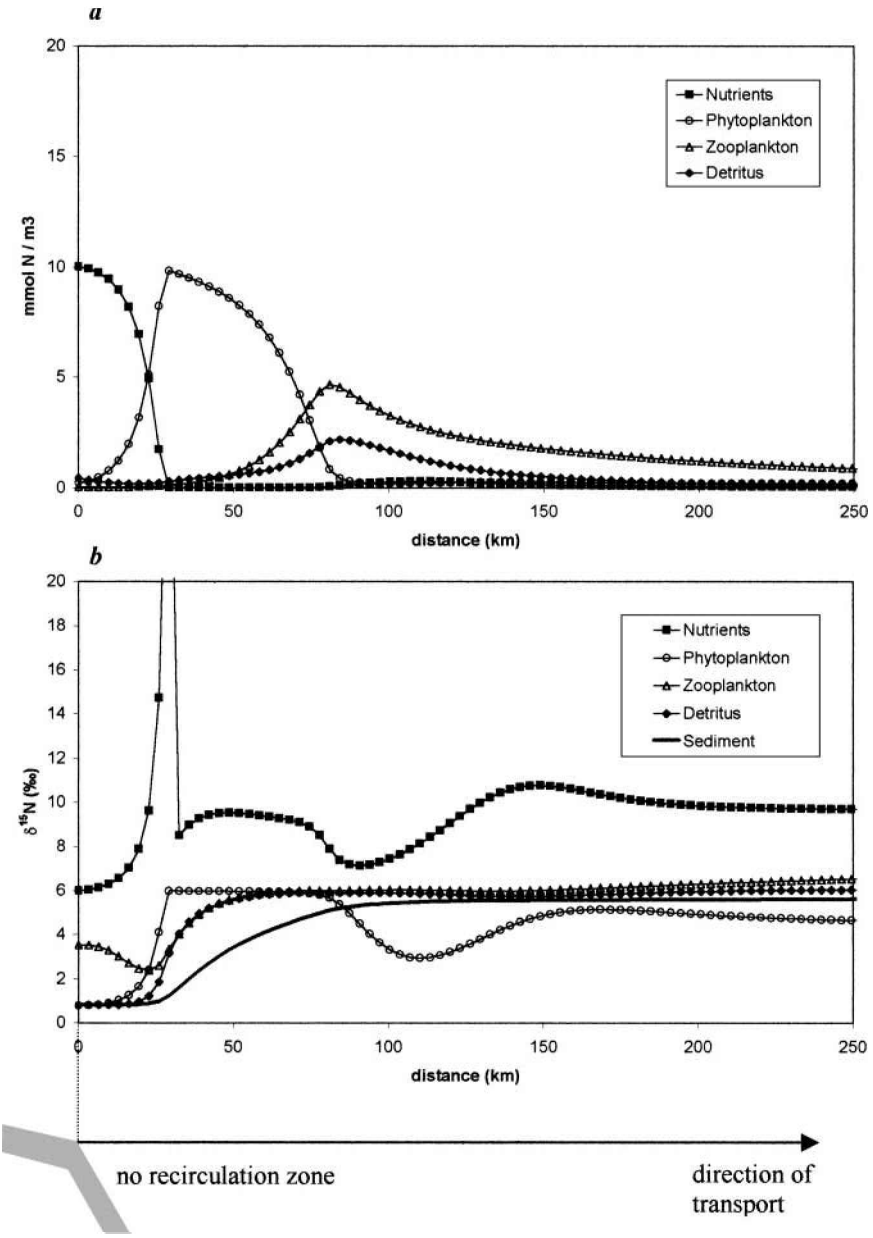

Figure 6. Evolution of the biological variables in a low sea level scenario. The cell length for the recirculation is 0 km. (a) Evolution of the concentrations, in mmol N m^{-3}. (b) Evolution of the $\delta^{15}N$, in ‰.

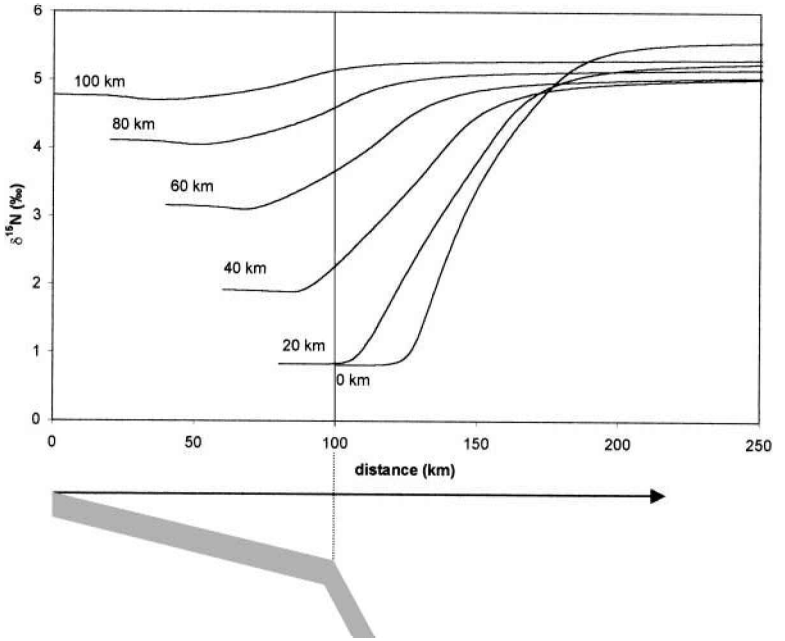

Figure 7. Sediment $\delta^{15}N$ curves for the different sea level scenarios. The recycling cell lengths (above each curve) range between 0 and 100 km. The origin point is the "actual coast point" (i.e. the upwelling emergence point) and x-axis is the distance offshore. The limit of recirculation is at 100 km.

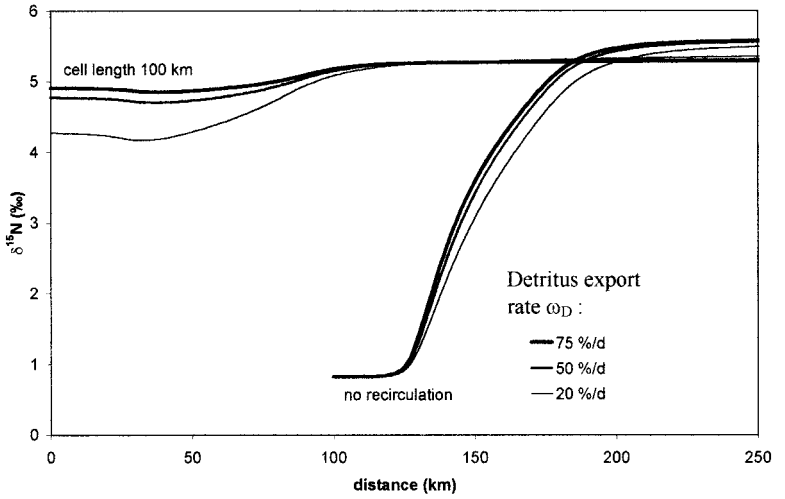

Figure 8. Influence of the export rate of detritus from the surface layer.

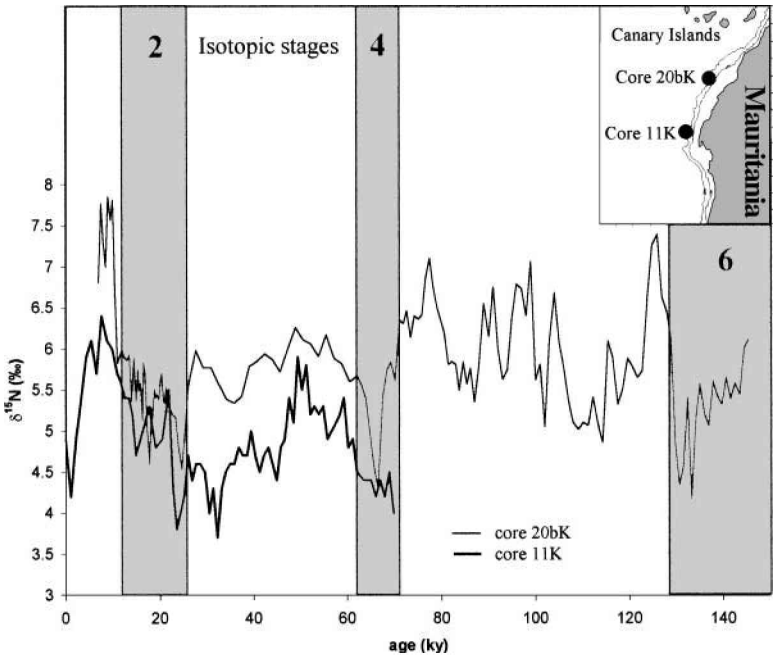

Figure 9. Evolution of $\delta^{15}N$ in the sedimentary cores 11K and 20bK (from Martinez, 1997).

c. Comparison with sediment data offshore of the Mauritanian upwelling

Figure 9 presents sediment $\delta^{15}N$ values obtained for two cores off Mauritania, collected during the SEDORQUA cruise. In both cores, the transition from glacial stage 2 to interglacial stage 1 is accompanied by an augmentation of the $\delta^{15}N$. This increase can be simulated by our model. During the low sea level scenario, the coring sites are close to the emergence point of the upwelling and correspond to the lower part of the sigmoid curve (Fig. 7, 0 km of recycling). Depending on the surface current speed and the sigmoid nature of the $\delta^{15}N$ curve, we can find a position on the curve to explain the lowest values, i.e. around 3.5‰. On the contrary, the high sea level scenarios of the model always induce higher values but not as high as the 7.5‰ observed in the data. However, the model is sensitive to the boundary conditions imposed and in particular to the value of the inflow at the bottom offshore box. If we set the $\delta^{15}N$ of those injected nutrients to 8.2‰ (instead of 6‰), we may obtain a range for the sediment $\delta^{15}N$ between 3‰ and 7.9‰ (Fig. 10), in good agreement with observations. We, therefore, reproduce the $\delta^{15}N$ increase according to the sea level rise. Another alternative to yield the observed $\delta^{15}N$ values could be to include a diagenetic enrichment relative to the near surface-generated signal as invoked by Altabet and François (1994) in the southern ocean south of the polar front.

The highest values of $\delta^{15}N$ appear during the transition and not at the climatic optimum. The core 11K shows a $\delta^{15}N$ decrease after this maximum whereas the sea level continues to rise. To reconstruct such a feature with the model, the flat curves we obtain for high sea

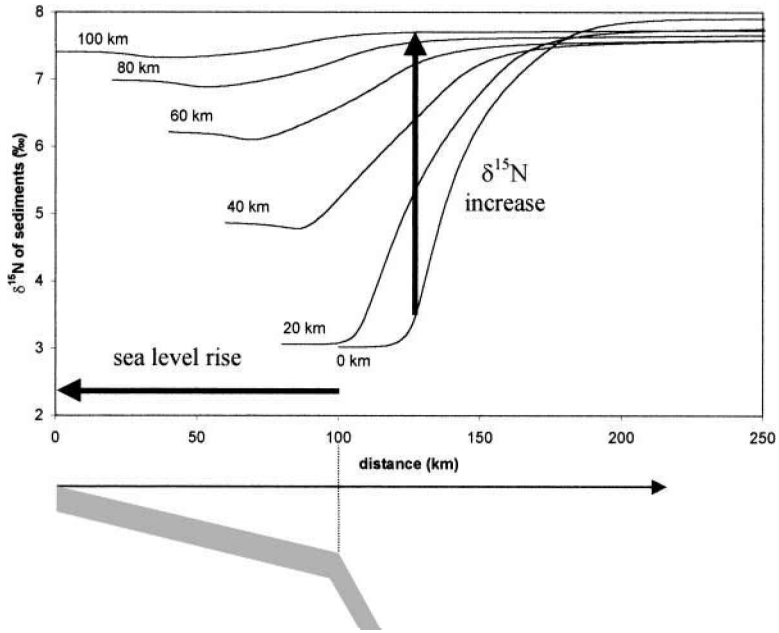

Figure 10. Sediment $\delta^{15}N$ curves for a nutrient inflow $\delta^{15}N$ set at 8.2‰. In comparison with Figure 7, this different input induces higher $\delta^{15}N$ values. The vertical arrow shows that for a determined coring site (relative to the actual emergence point, i.e. the origin of the *x*-axis) the translation of the $\delta^{15}N$ sediment curves, according to the sea level variations, can explain the increase of the $\delta^{15}N$ sedimentary record from the glacial to interglacial stages.

level must be lower than for some lower sea level. That is only the case for short cell length scenarios (i.e. low sea level) and the difference is not significant (0.5‰). With the present parameterization of the model, we can therefore reconstruct the upward slope of the curve during the glacial-interglacial transition, for both cores, but not the following decrease observed in many sites (Altabet *et al.,* 1995; Holmes *et al.,* 1997). Improvements can come with the modification of some forcing factors like surface current speed that may have changed along the glacial-interglacial periods.

Bertrand *et al.* (2000) have reproduced this drop after the maximum, using a less complex biological model, which did not integrate trophic levels. Here we show that this biological complexity is responsible for the particular behavior of the $\delta^{15}N$ sigmoid curve for low stand sea level scenarios. For the high sea level scenarios, as they did, we obtain a flat curve but with a high value, whereas they suggested lower values for high sea level conditions. With our model, only small cell length scenarios provide a decrease of sediment $\delta^{15}N$ with a rise of sea level. Maybe a more complex trophic chain would improve this possible drop of $\delta^{15}N$, by slowing down the mass transfer of nitrogen through the trophic levels.

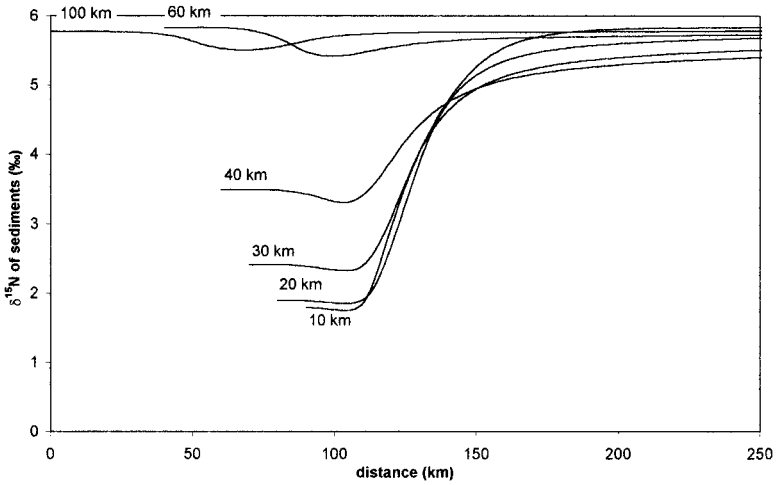

Figure 11. Sediment $\delta^{15}N$ curves for a recirculation configuration where export is higher in the shelf cell closure.

d. Effect of the shelf cell closure

In all previous runs, we neglected the closure of the continental shelf cell. However, the recirculation on the Mauritanian type shelf is a cell closed by vertical velocities at its offshore side (Fig. 3a). We investigate here its influence on the isotopic signature of detritus. In this configuration, to remain consistent with the standard recycling rate, we simply impose a spatial heterogeneity of the export rate. At the offshore side cell, ω_D is increased to 0.75 d^{-1} to simulate vertical velocities and kept constant at 0.2 d^{-1} all along the offshore transect.

We obtain the same kind of $\delta^{15}N$ sigmoid curves for low sea level scenarios and flat $\delta^{15}N$ curves for high sea level scenarios (Fig. 11). This cell closure increases the homogenization effect for the beginning of the $\delta^{15}N$ curves but it does not change the possible interpretation about the increasing $\delta^{15}N$ during the sea level rise.

The location of the cell closure according to the emergence of the upwelling plays an important role on the recirculation of the nutrients. The timing of the maximum planktonic growth with respect to the location of this front will not be the same if the front moves with the upwelling intensity or is at a fixed point upon the shelf break. This can be resolved by further understanding of the coastal upwelling systems as well as by a numerical study with a coupled model.

5. Conclusion

The simulation of the $\delta^{15}N$ variables in a simple NPZD biological model is possible using basic equations of isotope fractionation during photosynthesis and zooplankton excretion processes. In an upwelling configuration, with a development of the biology beginning with a strong input of nutrients and an evolution from an eutrophic to an

oligotrophic situation, the behavior of the $\delta^{15}N$ depends on the mass transfer of the nitrogen isotopes along the trophic chain. The resulting evolution curve for the sediment $\delta^{15}N$ is a sigmoid curve from the upwelling emergence point to the offshore, in the case of a narrow continental shelf recirculation, i.e. for low sea level scenarios as in the glacial periods. For the long continental cell length, the recirculation provides a homogenization effect, which leads to a flat $\delta^{15}N$ curve. These different curves for glacial and interglacial periods allow the reconstruction of the increase observed in core sediment $\delta^{15}N$ of the Mauritanian upwelling, without considering any diagenetic enrichment or nitrogen fixation/denitrification processes. Further work will couple our NPZD-$\delta^{15}N$ biological model with a primitive equation circulation model allowing us to test palaeoceanographic and palaeoclimatic scenarios for coastal upwelling areas.

Acknowledgments. We thank both anonymous reviewers for their very useful and constructive comments. Support for this work was provided by the Centre National de la Recherche Scientifique through the LEGOS and Groupement De Recherche (GDR 1187) PALEOPRO and by a grant from the Ministère de la Recherche through the UMR 5805 EPOC. Isotopic data were collected during the SEDORQUA oceanographic cruise on the Suroi and measured at the University of Vancouver (T. Pedersen, S. Calvert).

REFERENCES

Alldredge, A. L. and C. Gotschalk. 1988. *In situ* settling behavior of marine snow. Limnol. Oceanogr., *33,* 339–351.

Altabet, M. A. 1988. Variations in nitrogen isotopic composition between sinking and suspended particles: implications for nitrogen cycling and particle transformation in the open ocean. Deep Sea Res., *35,* 535–554.

Altabet, M. A. and W. B. Curry. 1989. Testing models of past ocean chemistry using foraminifera 15N/14N. Global Biogeo. Cycles, *3,* 107–119.

Altabet, M. A. and R. François. 1994. Sedimentary nitrogen isotopic ratio as a recorder for surface ocean nitrate utilization. Global Biogeo. Cycles, *8,* 103–116.

Altabet, M. A., R. François, D. W. Murray and W. L. Prell. 1995. Climate-related variations in denitrification in the Arabian Sea from sediment 15N/14N ratios. Nature, *373,* 506–509.

Babin, M., A. Morel, H. Claustre, A. Bricaud, Z. Kolber and P. G. Falkowski. 1996. Nitrogen- and irradiance-dependent variations of the maximum quantum yield of carbon fixation in eutrophic, mesotrophic and oligotrophic marine systems. Deep-Sea Res. Part I, *43,* 1241–1272.

Bertrand, P., P. Martinez, S. Calvert, T. Pedersen and G. Shimmield. 2000. Sea level impact on nutrient cycling in coastal upwelling areas during deglaciation: evidence from nitrogen isotopes. Global Biogeo. Cycles, *14,* 341–356.

Calvert, S. E., C. A. Baturin-Pollock, J. W. Farrell, R. S. Ganeshram, T. F. Pedersen, N. A. D. Waser and J.-P. Wu. 1995. Nitrogen isotope ratios in sedimentary organic matter as a proxy for nutrient utilization and palaeoproductivity, *in* Organic Geochemistry: Developments and Applications to Energy Climate, Environments and Human History, Grimalt and Dorronsoro, eds., 880–881.

Calvert, S. E., B. Nielsen and M. R. Fontugne. 1992. Evidence from nitrogen isotope ratios for enhanced productivity during formation of eastern Mediterranean sapropels. Nature, *359,* 223–225.

Checkley, D. M. J. and C. A. Miller. 1989. Nitrogen isotope fractionation by oceanic zooplankton. Deep-Sea Res., *36,* 1449–1456.

Chen, D. and D.-P. Wang. 1990. Simulating the time-variable coastal upwelling during CODE 2. J. Mar. Res., *48,* 335–358.

DeNiro, M. J. and S. Epstein. 1980. Influence of diet on the distribution of nitrogen isotopes in animals. Geochim. Cosmochim. Acta, *45,* 341–351.

Evans, G. 1999. The role of local models and data sets in the Joint Global Ocean Flux Study. Deep-Sea Res. I, *46,* 1369–1389.

Falkowski, P. G. 1997. Evolution of the nitrogen cycle and its influence on the biological sequestration of CO2 in the ocean. Nature, *387,* 272–275.

Farrell, J. W., T. F. Pedersen, S. E. Calvert and B. Nielsen. 1995. Glacial-interglacial changes in nutrient utilization in the Equatorial Pacific Ocean. Nature, *377,* 514–517.

Fogel, M. L. and L. A. Cifuentes. 1993. Isotope Fractionation during Primary Production, *in* Organic Geochemistry, M. H. Engel and A. Macko, eds., Plenum Press, NY, 73–98.

Fraga, F. 1974. Distribution des masses d'eau dans l'upwelling de Mauritanie. Tethys, *6,* 5–10.

François, R., M. A. Altabet and L. H. Burckle. 1992. Glacial to interglacial changes in surface nitrate utilization in the Indian sector of the Southern Ocean as recorded by sediment d15N. Paleoceanography, *7,* 589–606.

Ganeshram, R. S., T. F. Pedersen, S. E. Calvert and J. W. Murray. 1995. Large changes in oceanic nutrient inventories from glacial to interglacial periods. Nature, *376,* 755–758.

Holmes, M. E., P. J. Müller, R. R. Schneider, M. Segl, J. Pätzold and G. Wefer. 1996. Stable nitrogen isotopes in Angola Basin surface sediments. Mar. Geol., *134,* 1–12.

Holmes, M. E., P. J. Müller, R. R. Schneider, M. Segl and G. Wefer. 1998. Spatial variations in euphotic zone nitrate utilization based on delta N-15 in surface sediments. Geo-Mar. Lett., *18,* 58–65.

Holmes, M. E., R. R. Schneider, P. J. Müller, M. Segl and G. Wefer. 1997. Reconstruction of past nutrient utilization in the eastern Angola Basin based on sedimentary 15N/14N ratios. Paleoceanography, *12,* 604–614.

Jacques, G. and P. Tréguer. 1986. Ecosystèmes Pélagiques Marins, Masson, 243 pp.

Liu, K.-K. and I. R. Kaplan. 1989. The eastern tropical Pacific as a sources of 15N-enriched nitrate in seawater off southern California. Limnol. Oceanogr., *34,* 820–830.

Martinez, P. 1997. Paléoproductivités du système d'upwellings nord-ouest africain et variations climatiques au cours du Quaternaire terminal. PhD thesis, Bordeaux I, 297 pp.

Martinez, P., P. Bertrand, S. E. Calvert, T. F. Pedersen, G. B. Shimmield and E. Lallier-Vergès. 2000. Spatial variations in nutrient utilization, production and diagenesis in the sediments of coastal upwelling regime (NW Africa): Implications for palaeoceanographic record. J. Mar. Res., *58,* (in press).

Minagawa, M. and E. Wada. 1984. Stepwise enrichment of 15N along food chains: Further evidence and the relation between d15N and animal age. Geochim. Cosmochim. Acta, *48,* 1135–1140.

Minas, H. J., L. A. Codispoti and R. C. Dugdale. 1982. An analysis of production-regeneration system in the coastal upwelling area of NW Africa based on oxygen, nitrate and ammonium distributions. J. Mar. Res., *40,* 615–641.

Mittelstaedt, E. 1991. The ocean boundary along the northwest Africa coast: Circulation and oceanographic properties at the sea surface. Prog. in Oceanogr., *26,* 307–355.

Montoya, P. 1994. Nitrogen isotope fractionation in the modern ocean: implication for sedimentary record, *in* Carbon Cycling in the Glacial Ocean: Constraints on the Ocean's Role in Global Change, R. Zahn, ed., Berlin Heidelberg, 259–279.

Neumann, G. 1968. Ocean Currents, 4, Elsevier Publishing Company, Amsterdam—London—New York, 351 pp.

Oschlies, A. and V. Garçon. 1998. Eddy-induced enhancement of primary production in a model of North Atlantic Ocean. Nature, *394,* 266–269.

—— 1999. An eddy-permitting coupled physical-biological model of the North Atlantic—1. Sensitivity to advection numerics and mixed layer physics. Global Biogeo. Cycles, *13,* 135–160.

Pietrafesa, L. J. 1983. Shelfbreak circulation, fronts and physical oceanography: east and west coast perspectives, *in* The Shelfbreak: Critical Interface on Continental Margins, D. Stanley and G. Moore, eds., Society of Economic Paleontologists and Mineralogists, Tulsa, Oklahoma, USA, 233–250.

SCOR, W. G. 1975. Report of the second meeting on coastal upwelling processes, 10, Proc. Sci. Com. Oceanic Res., Kiel F.R.G.

Smith, R. L. 1995. The physical processes of coastal ocean upwelling systems, *in* Upwelling in the Ocean: Modern Processes and Ancient Records, C. P. Summerhayes, K.-C. Emeis, M. V. Angel and B. Zeitschel, eds. John Wiley & Sons, 39–64.

Steele, J. H. and E. W. Hederson. 1992. The role of predation in plankton models. J. Plank. Res., *14,* 157–172.

Voss, M., M. A. Altabet and B. Vonbodungen. 1996. d15N in sedimenting particles as indicator of euphotic-zone processes. Deep-Sea Res. Part I, *43,* 33–47.

Waser, N. A. D., P. J. Harrison, B. Nielsen, S. E. Calvert and D. H. Turpin. 1998. Nitrogen isotope fractionation during the uptake and assimilation of nitrate, nitrite, ammonium and urea by a marine diatom. Limnol. Oceanogr., *43,* 215–224.

Wefer, G. and G. Fischer. 1993. Seasonal patterns of vertical particle flux in equatorial and coastal upwelling areas of the eastern Atlantic. Deep-Sea Res. I, *40,* 1613–1645.

Werner, F. E. 1987. A numerical study of secondary flows over continental shelf edges. Cont. Shelf Res., *7,* 379–409.

Received: *10 August, 1999;* revised: *7 March, 2000.*